Catena 206 (2021) 105577

Contents lists available at ScienceDirect

Catena

journal homepage: www.elsevier.com/locate/catena

An in-depth statistical analysis of the rainstorms erosivity in Europe

Nejc Bezak [a,*], Matjaž Mikoš [a], Pasquale Borrelli [b,c], Leonidas Liakos [d], Panos Panagos [d]

[a] University of Ljubljana, Faculty of Civil and Geodetic Engineering, Slovenia
[b] Department of Earth and Environmental Sciences, University of Pavia, Italy
[c] Department of Biological Environment, Kangwon National University, Chuncheon 24341, Republic of Korea
[d] European Commission, Joint Research Centre (JRC), Ispra, Italy

ARTICLE INFO

Keywords:
Rainfall erosivity
REDES
Lorenz curve
Gini coefficient
Seasonality
Threshold values
R-factor
Europe

ABSTRACT

Heavy rainstorms play a central role in the water-driving soil erosion processes. An in-depth knowledge about temporal and spatial erosivity of rainfall events is required to gain a better understanding of soil erosion processes and optimize soil protection measures efficiency. In this study, the spatiotemporal distribution of more than 300,000 erosive events measured at 1181 locations, part of the Rainfall Erosivity Database at European Scale (REDES) database, is studied to shed some new light on the rainfall erosivity in Europe. Rainfall erosive events are statistically investigated through the Lorenz curve and derived coefficients such as the Gini coefficient (G). Additionally, seasonal characteristics of the most and the less erosive events are compared to investigate seasonal characteristics of rainstorms across Europe. The G shows largest values of inequality of the inter-annual temporal distribution of the rainfall erosive events in the Alpine region, mostly due to the large number of rainfall events with smaller rainfall erosivity. While for other parts of Europe, the inequality described by the G is mostly due to a small number of high erosive events. The G slightly decreases from south to north while no clear regional patterns can be detected. Additionally, in Europe, on average 11% (ranging from 1 to 24%) of all erosive events contribute to form 50% of the total rainfall erosivity. Furthermore, higher erosive rainfall events tend to occur later in the year compared to less erosive events that take place earlier. To our knowledge, this study is the first one addressing event scale rainfall erosivity distribution using more than 300,000 rainfall erosivity events and covering almost a whole continent. Scientifically our findings represent a major step towards large-scale process-based erosion modelling while, practically, they provide new elements that can support national and local soil erosion monitoring programs.

1. Introduction

Erosion by water is considered as one of the leading causes of land degradation and an important environmental hazard. Contemporary studies conducted in Europe and other continents pointed out that this type of erosion is probably the most frequently studied and can yield high erosive rates (Bezak et al., 2021b; Borrelli et al., 2021, 2017; Lukić et al., 2019, 2018b, 2016; Panagos et al., 2015b). Rainfall erosivity is an index that quantitatively describes the water-driving force for soil erosion (Nearing et al., 2017; Panagos et al., 2015a). It is often regarded as one of the most important factors affecting the spatial and temporal variability of several soil erosion displacement processes such as gullying, sheet and rill erosion, subsurface erosion and landslides (Almagro et al., 2017; Beguería et al., 2018; Bezak et al., 2020, 2015b; Borrelli et al., 2016; Ferro et al., 2020; Panagos et al., 2016a). Expressed as the product of the total kinetic energy of a rainfall event times its 30-minute maximum rainfall intensity (Wischmeier and Smith, 1978), its accurate calculations requires high-resolution pluviographic data (ideally 5-minute time step), which are generally not available over large study areas and time periods (Petek et al., 2018). Accordingly, frequently available daily and monthly rainfall data are generally used (Beguería et al., 2018; Liu et al., 2020). Especially while performing large-scale assessments, such as the continental ones, where the aim is to identify potential soil erosion risk areas and to support the development of field scale observations and mitigation strategies (Liu et al., 2020).

Furthermore, national or regional data providers often cannot provide large amounts of high-resolution precipitation data, or cannot provide them free of charge. Therefore, a database resulting from collaborative research activities such as the Rainfall Erosivity Database at European Scale (REDES) that includes rainfall erosive event

* Corresponding author at: Jamova 2, 1000 Ljubljana, Slovenia.
E-mail address: nejc.bezak@fgg.uni-lj.si (N. Bezak).

https://doi.org/10.1016/j.catena.2021.105577
Received 3 February 2021; Received in revised form 3 June 2021; Accepted 1 July 2021
Available online 9 July 2021

information from more than 1500 European stations (Ballabio et al., 2017; Bezak et al., 2020; Panagos et al., 2017, 2016b), constitute a suitable option for regional and continental scale studies. In addition, being based on sub-hourly and hourly records, REDES allows to investigate the characteristics of rainfall erosive events. Alternatively, one could use high-resolution-satellite-based precipitation products instead of interpolating ground-based rain-gauge observations (Kim et al., 2020). The topic is of great importance since erosive rainfall may further increase in both frequency and intensity due to climate change (Borrelli et al., 2020) and several open questions need to be further addressed to enhance knowledge about erosion processes.

Different studies have investigated characteristics of rainfall erosive events at smaller scales in Europe such as Switzerland (Meusburger et al., 2012), Italy (Borrelli et al., 2016), Calabria (Capra et al., 2017), Greece (Panagos et al., 2016a), island of Crete (Grillakis et al., 2020), Slovenia (Petek et al., 2018), Netherlands (Lukić et al., 2018a), a large basin including parts of Serbia, Hungary and Croatia (Lukić et al., 2019, 2016) and NE Spain (Angulo-Martínez and Beguería, 2012), among others. Some studies have also analyzed seasonal and monthly characteristics of rainfall erosivity (Angulo-Martínez and Beguería, 2012; Borrelli et al., 2016; D'Asaro et al., 2007; Meusburger et al., 2012; Panagos et al., 2016a; Vallebona et al., 2015). Ballabio et al. (2017) used the REDES database to analyze the monthly rainfall erosivity characteristics in Europe but without observing the seasonal dynamics and contributions of the most erosive events. Several other studies were performed on this topic outside Europe, the most recent ones include a study about climate change impact on erosivity in Brazil (Almagro et al., 2017), analyzing the spatiotemporal variability in rainfall erosivity in mainland China for the period 1960–2018 (Chen et al., 2020), in the Loess Plateau of China for the period 1971–2010 (Cui et al., 2020), and at the continental scale in the United States for the period 1998–2015 using a high-resolution-satellite-based precipitation data (Kim et al., 2020) or at the global scale for the period 1980–2017 using daily precipitation data (Liu et al., 2020).

Rainfall erosivity at continental scale is highly variable in space and time (Ballabio et al., 2017; Bezak et al., 2020; Panagos et al., 2015a). Accordingly, further in-depth knowledge about the temporal and spatial distribution of heavy rainfall events is needed to better address soil erosion and its related environmental and economic issues (Lal, 1998). A possible approach to effectively describe the temporal distribution and variability of rainfall erosive events at a station level may be represented by the use of the Lorenz curve (Lorenz, 1905; Masaki et al., 2014); which is frequently applied in economics studies to represent the inequality of the wealth distribution in a society (Lorenz, 1905). This concept has been applied to the environmental data multiple times (e.g., Jawitz and Mitchell, 2011; Masaki et al., 2014; Shi et al., 2013) and multiple authors have stated that the Lorenz curve is an effective way of assessing rainfall distribution (Shi et al., 2013). Therefore it can also be used to assess rainfall erosivity distribution. Based on the Lorenz curve, different scalar measures of inequality such as Gini coefficient (G) (Gini, 1914) or Lorenz coefficient of asymmetry (LA) can be calculated to analyze the temporal distribution characteristics presented by the Lorenz curve. As pointed out by some studies, the Gini coefficient as a single scalar value can be an insufficient measure of inequality presented by a Lorenz curve (Clementi et al., 2019; Tarsitano, 1988). Therefore, additional coefficient such as Lorenz coefficient of asymmetry can be applied. Approaches based on Lorenz curve were applied in numerous other fields such as ecology (Damgaard and Weiner, 2000) and hydrology (Jawitz and Mitchell, 2011; Masaki et al., 2014), among others. These coefficients have been quite frequently applied to various hydrological problems such as temporal distribution of river discharge (Jawitz and Mitchell, 2011; Masaki et al., 2014) or analyzing precipitation characteristics (Martin-Vide, 2004; Monjo and Martin-Vide, 2016; Rajah et al., 2014; Royé and Martin-Vide, 2017; Sangüesa et al., 2018; Shi et al., 2013; Sun et al., 2017; Yin et al., 2016). However, to the best of our knowledge, investigation of temporal variability of rainfall erosivity using the Lorenz curve, and its scalar measures, have not yet been attempted; not even at regional or local scale. Thus, the Lorenz curve can provide a graphical view of the cumulative percentage of erosive rainfall events and G and LA can provide an explanation of the underlying inequalities in the distribution of erosive rainfall events (Shi et al., 2013).

Among others, the focus is to explore and address the following research questions: a) what is the distribution and frequency of the most erosive rainfall events in comparison to less erosive rainfall events; b) what is the percentage of erosive rainfall events that contribute to the 50% of the total annual erosivity; c) what are the seasonal characteristics of the most erosive rainfall events and d) how do these characteristics change across Europe. The 50% threshold was also used by González-Hidalgo et al. (2009) when studying effect of the largest events on the total soil loss. In order to answer these questions, the temporal distribution and the seasonal characteristics of the rainfall erosive events have to be studied at the continental scale. As a first step, a preliminary study of the temporal distribution of rainfall erosive events at the station level was conducted. It comes as no surprise that erosive rainfall erosivity events at precipitation (gauging) measuring stations are not evenly distributed throughout the year (Angulo-Martínez and Beguería, 2012; Meusburger et al., 2012). A conspicuous number of observations across the earth confirmed that a few (i.e. up to 10–15%) heavy rainstorms are responsible for the large part of annual rainfall erosivity (Borrelli et al., 2016; Meusburger et al., 2012; Petek et al., 2018) and consequently also for the larger part of the total soil erosion rates (Bagarello et al., 2011; González-Hidalgo et al., 2009). As a consequence, a mere counting of rainfall erosive events does not say much about the actual annual rainfall erosivity that is important to estimate soil loss or land degradation due to soil erosion (Borrelli et al., 2020; Panagos et al., 2015b; Yin et al., 2017).

Therefore, the overall aim of this study is to enhance the current knowledge on rainfall erosive events characteristics at the European scale by introducing the analysis of the Lorenz curves including two scalar measures of their unequal distribution: i.e., Gini coefficient (G) and Lorenz asymmetry coefficient (LA). In addition, a further aim of this study is to propose novel indicators of rainfall erosivity to more comprehensively address its spatiotemporal distribution and patterns since scalar measures such as G can capture the variability in the distribution of rainfall erosive events and express it with a numeric value.

In the scope of the presented paper, the following hypothesis are investigated: (i) in Europe, different spatial patterns of Gini coefficient (G) calculated based on the erosive rainfall event data can be observed; (ii) the derived G can be related to the total annual rainfall erosivity; (iii) the share of the rainfall erosive events that contribute to the 50% of the total erosivity changes across Europe; (iv) seasonal characteristics of the most erosive rainfall events are significantly different than those of all other rainfall erosive events, and (v) stations showing similar G values may significantly differ in the Lorenz asymmetry coefficient (LA), as a result of their different heterogeneity. The data used and the methodology applied to address these hypotheses are presented in the following section.

2. Data and methods

2.1. REDES database and derived products

The Rainfall Erosivity Database at European scale (REDES) is the result of a collaborative effort to collect sub-hourly and hourly rainfall data across EU Member states and Switzerland (Ballabio et al., 2017; Panagos et al., 2017, 2015a). Based on the detailed rainfall records collected for 1675 stations, the rainfall erosivity values of each erosive storm were calculated (Panagos et al., 2015a). Afterwards, these were aggregated to form monthly and annual values. Accordingly, the REDES database includes three main components: i) the rainfall erosivity values of each single rainfall erosive event (including date, rain [mm], duration [h] and maximum intensity [mm/h]), ii) mean monthly values of

Table 1
Overview of studies that used REDES database with some basic information.

Study area	Temporal scale	Observed period	Spatial interpolation	Reference
Switzerland	Annual	Present	Regression-kriging	(Meusburger et al., 2012)
EU-28	Annual	Present	Gaussian Process Regression	(Panagos et al., 2015a)
Greece	Annual	Present	Generalised Additive Model	(Panagos et al., 2016a)
EU-28	Monthly	Present	Gaussian Process Regression	(Panagos et al., 2016b)
Italy	Rainstorms/ monthly	Present	Regression-kriging	(Borrelli et al., 2016)
EU-28	Monthly	Present	Gaussian Process Regression	(Ballabio et al., 2017)
EU-28	Annual	Future	Gaussian Process Regression	(Panagos et al., 2017)
EU-28	Annual	Past/ present	Gaussian Process Regression	(Bezak et al., 2020)
EU-27 + UK	Annual	Present	–	(Bezak et al., 2021a)
EU-27 + UK	Rainstorms	Present	–	Current study

rainfall erosivity, and iii) mean annual values of rainfall erosivity. The annual erosivity is publicly available for 1675 stations and the monthly erosivity is available for 1567 stations (total: 18,804 records of mean monthly values). The conversion factors (Panagos et al., 2016b) were used in order to harmonize different temporal data resolution (5- to 60-min) to a temporal resolution of 30-min.

Aggregating the single rainfall erosive events, the six rainfall erosivity clusters that were derived using the K-means methodology were mapped (Ballabio et al., 2017). An overview of multiple applications based on the REDES database is shown in Table 1. The main idea of applying the K-means clustering method to the monthly rainfall erosivity maps is to obtain an optimal number of relatively homogenous areas from the seasonal rainfall erosivity perspective (Ballabio et al., 2017). Thus, as a result six homogeneous areas were identified (Ballabio et al., 2017). Cluster (i.e. zone) 1 covers areas of Eastern Europe while clusters 2 and 3 cover larger part of EU (Northern and Western Europe). Cluster 4 includes major parts of the Southern Europe while cluster 5 is limited to parts of United Kingdom, France, etc. Cluster 6 is the smallest and is limited to the Alpine region. Thus, every cluster zone is characterized by distinct seasonal erosivity characteristics (Ballabio et al., 2017). Therefore, the K-means cluster map is also used in this study to provide new knowledge about erosivity characteristics in different parts of Europe.

With the exception of Italy (Borrelli et al., 2016), the characteristics of the single REDES rainfall erosive events have not been explored in detail so far. Due to data access limitations and privacy issues, the single rainfall erosive events records data are available for 1181 gauging stations (71% of the REDES database). Nevertheless, REDES currently hosts detailed information for more than 300,000 rainfall erosive events. This means that more than 250 rainfall erosive events per station is available, distributed over the period 1953–2014. The pluviographic records cover periods ranging from a minimum of three years to a maximum of 72 years, with an average period of around 16 years. Furthermore, it should be noted that rainfall erosive events in the REDES database were identified according to the RUSLE methodology (Renard et al., 1997) where

Table 2
A hypothetical distribution of the 10 erosive events with total erosivity of 1000 MJ mm $ha^{-1}h^{-1}$ and the corresponding values of Gini coefficient (G), Shannon entropy (H) and Lorenz asymmetry coefficient (LA).

Case	Rainfall erosivity events [MJ mm $ha^{-1}h^{-1}$]	G	H	LA
1	977, 2, 1, 2, 3, 4, 5, 1, 2, 3	0.88	0.23	1.03
2	770, 20,10,20,30,40,50,10,20,30	0.73	1.47	1.19
3	98,102,97,103,95,105,100,100,92,108	0.03	3.32	0.98
4	20,130,191,50,1,30,90,160,60,268	0.45	2.82	0.91
5	1,2,4,3,5,185,210,185,205,200	0.50	2.43	0.67
6	10,20,40,30,50,160,190,165,185,150	0.39	2.90	0.78

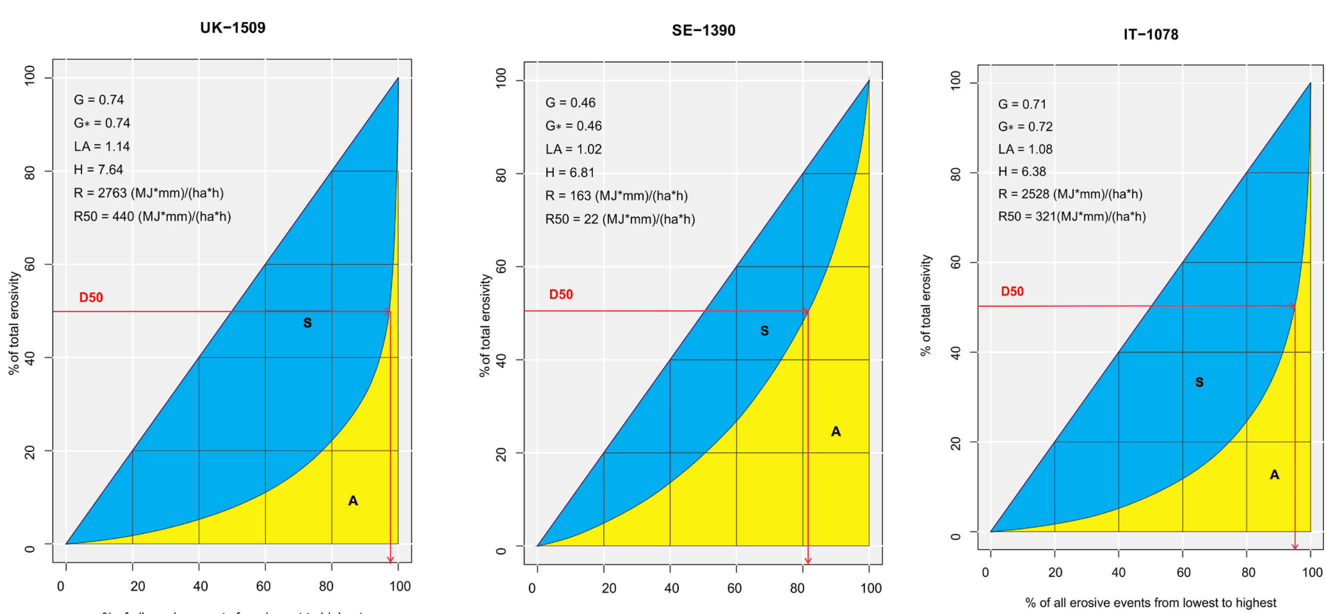

Fig. 1. Three examples of Lorenz curves (i.e. black line) and calculated Gini coefficients (G), normalized Gini coefficients (G*), Shannon entropy (H), Lorenz asymmetry coefficient (LA), total annual rainfall erosivity (R) and R50 threshold (Section 2.3) for all rainfall erosive events for selected three stations that are included in the REDES database. One station from United Kingdom (UK) (i.e. Moor House), station from Sweden (SE) (Overkalix-Svartbyn) and station from Italy (IT) (Taverna) are shown. Blue line indicates line of perfect equality. The red line indicates the D50 threshold value (Section 2.3). The station numbers are the IDs in the REDES database (e.g. UK1509 is the REDES ID = 1509). The definitions of S (i.e. blue area) and A (i.e. yellow area) are provided in relation to Eq. (2). (For interpretation of the references to colour in this figure legend, the reader is referred to the web version of this article.)

Table 3
Main descriptive statistics of Gini coefficients (G), Lorenz asymmetry coefficients (LA) and Shannon entropy (H) for all 1181 stations. Mean values are marked as bold text. Possible ranges of G, LA and H values are also provided.

Gini coefficient (G) [0,1]	Minimum	0.4
	25th percentile	0.57
	Mean	**0.61**
	75th percentile	0.65
	Maximum	0.78
	Standard deviation	0.06
Lorenz asymmetry coefficient (LA) [0,2]	Minimum	0.84
	25th percentile	1.00
	Mean	**1.04**
	75th percentile	1.08
	Maximum	1.22
	Standard deviation	0.06
Shannon entropy (H) [0,∞)	Minimum	2.80
	25th percentile	5.76
	Mean	**6.44**
	75th percentile	7.07
	Maximum	10.82
	Standard deviation	1.1

Table 4
Basic statistics of Gini coefficients (G), Lorenz asymmetry coefficients (LA) and Shannon entropy (H) for different K-means clusters as defined by Ballabio et al. (2017). Mean values are marked as bold text.

	K-means cluster	1	2	3	4	5	6
Gini coefficient (G)	Minimum	0.44	0.42	0.40	0.45	0.48	0.62
	Mean	**0.63**	**0.59**	**0.60**	**0.62**	**0.63**	**0.69**
	Maximum	0.75	0.75	0.78	0.77	0.76	0.78
Lorenz asymmetry coefficient (LA)	Minimum	0.88	0.84	0.90	0.88	0.93	0.94
	Mean	**1.03**	**1.06**	**1.06**	**1.02**	**1.02**	**0.97**
	Maximum	1.16	1.21	1.22	1.16	1.14	1.01
Shannon entropy (H)	Minimum	3.97	2.8	2.86	3.84	3.78	6.67
	Mean	**6.58**	**5.92**	**6.36**	**6.57**	**6.76**	**7.61**
	Maximum	9.41	9.45	9.97	10.82	9.78	8.53

detailed description is provided by Panagos et al. (2015a).

Similarly as Bezak et al. (2021a) that investigated the drivers of the rainfall erosivity synchrony scale in Europe, in this study the same datasets (listed below) are used in order to investigate the drivers of the diverse rainfall erosivity characteristics that can be found in Europe and can be described using the Lorenz curve. Additional climatic data used in this analysis are (i) data obtained from the European Centre for Medium-Range Weather Forecasts (ECMWF), namely convective precipitation (CP; accumulated rain and snow as part of the convection scheme in the ECMWF), convective available potential energy (CAPE; indicator of the instability of the atmosphere), large-scale precipitation (LSP; accumulated rain and snow as part of the cloud scheme in the ECMWF) and large-scale precipitation fraction (LSPF; accumulation of the LSP in the specific grid box), ii) the map of annual number thunderstorm days in Europe (Enno et al.,2020) as an indicator of the thunderstorm frequency, and iii) the erosivity synchrony scale estimates (Bezak et al., 2021a). Detailed description of these datasets can be found in Bezak et al. (2021a). The idea behind using these datasets is to evaluate if any of these can be regarded as an important driver of the erosivity characteristics that can be described using the Lorenz curve and its derived scalar measures.

2.2. Lorenz curve, Gini coefficient and Shannon entropy

In order to investigate the temporal distribution of the REDES rainfall erosive events across Europe, the Lorenz curve (Lorenz, 1905), non-dimensional Gini coefficient (G) (Gini, 1914), Lorenz asymmetry coefficient (LA) (Tarsitano, 1988), normalized Gini coefficient (G*) and Shannon entropy (H) coefficient (Shannon, 1948) are calculated. Those coefficients have already found wide acceptance in hydrological research (Ceriani and Verme, 2012; Damgaard and Weiner, 2000; Jawitz and Mitchell, 2011; Masaki et al., 2014). As pointed out by Masaki et al. (2014), the Lorenz curve and its parameters (scalar measures) are not only useful for the quantitate evaluation of the rainfall erosivity but also for graphical expression of the rainfall erosivity patterns across larger geographical units, such as Europe in our study. The Lorenz curve relates the accumulation of the selected variable and its cumulative frequency (Jawitz and Mitchell, 2011; Monjo and Martin-Vide, 2016) and can be according to Gastwirth (1971) be expressed as:

$$L(p) = \int_0^p F^{-1}(t)dt/\mu \tag{1}$$

In case that one assumes that X is a random variable with the cumulative distribution function (cdf) F(x) and $F^{-1}(t)$ is the inverse (Gastwirth, 1971). Thus, the Lorenz curve L(p) corresponds to any random variable with cdf and finite mean μ (Gastwirth, 1971). Based on the derived Lorenz curve, the G can be calculated as the ratio of (Jawitz and Mitchell, 2011; Monjo and Martin-Vide, 2016):

- area between the line of perfect equality and the Lorenz curve (S as shown in Fig. 1);
- area under the line of the perfect equality (S + A as shown in Fig. 1).

Graphical examples of the Lorenz curve and corresponding G can be seen in Fig. 1. According to the notions used in Fig. 1, G can be calculated as (Monjo and Martin-Vide, 2016):

$$\mathrm{G} = \mathrm{S}/(S+A) \tag{2}$$

where S and A can both be in the range between 0 and ½, and the G between 0 and 1. The value of the G close to 1 indicates significant inequality (A goes to 0), while a G value close to 0 (S goes to 0) indicates no inequality. In terms of rainfall erosivity, a G value of 0 indicates that all single rainfall erosive events have similar erosivity (i.e. no seasonal variation), while a G value close to 1 indicates that there is a range of erosivity with clear difference between more and less erosive rainfall events. Three examples of the Lorenz curve, corresponding G and normalized Gini coefficients (G*) are shown (Fig. 1). The normalization is used to define the G*. As shown in Fig. 1, G and G* are almost identical for the case of the rainfall erosivity.

The H can be used to assess the variability in environmental data such as rainfall or discharge (Mishra et al., 2009; Rodrigues da Silva et al., 2016, 2017) and is also calculated using rainfall erosivity data in this study. The H (Cowell, 2000; Jost, 2006; Shannon, 1948) is a measure of information (in bits) where more information results in lower entropy and vice versa (Mishra and Ayyub, 2019; Rodrigues da Silva et al., 2016; Shannon, 1948). To access the diversity of rainfall erosivity, richness would be a measure of the number of different classes of rainfall erosivity present at a rainfall gauging station, and evenness compares the similarity of the number of rainfall events in each of erosivity classes. Hence, a system (one rainfall station) with a high degree of richness and evenness would have a higher entropy, whereas a system (another rainfall station) with low degree of richness and evenness would have a low entropy. As a consequence, a system with high richness but low evenness would have a lower entropy than a system with high richness and high evenness (Rajaram et al., 2017). The H has been used to rethink diversity within probability distributions, based on the notion of information and can be expressed as (Mishra et al., 2009; Rodrigues da Silva et al., 2016; Shannon, 1948; Signorell, 2020):

$$H = -\sum(\pi log(\pi)) \tag{3}$$

where π is the probability of discrete random variable to occur, H is a measure of information in bits (less information results in higher entropy and vice versa) and H ranges from 0 to ∞ (Rodrigues da Silva et al.,

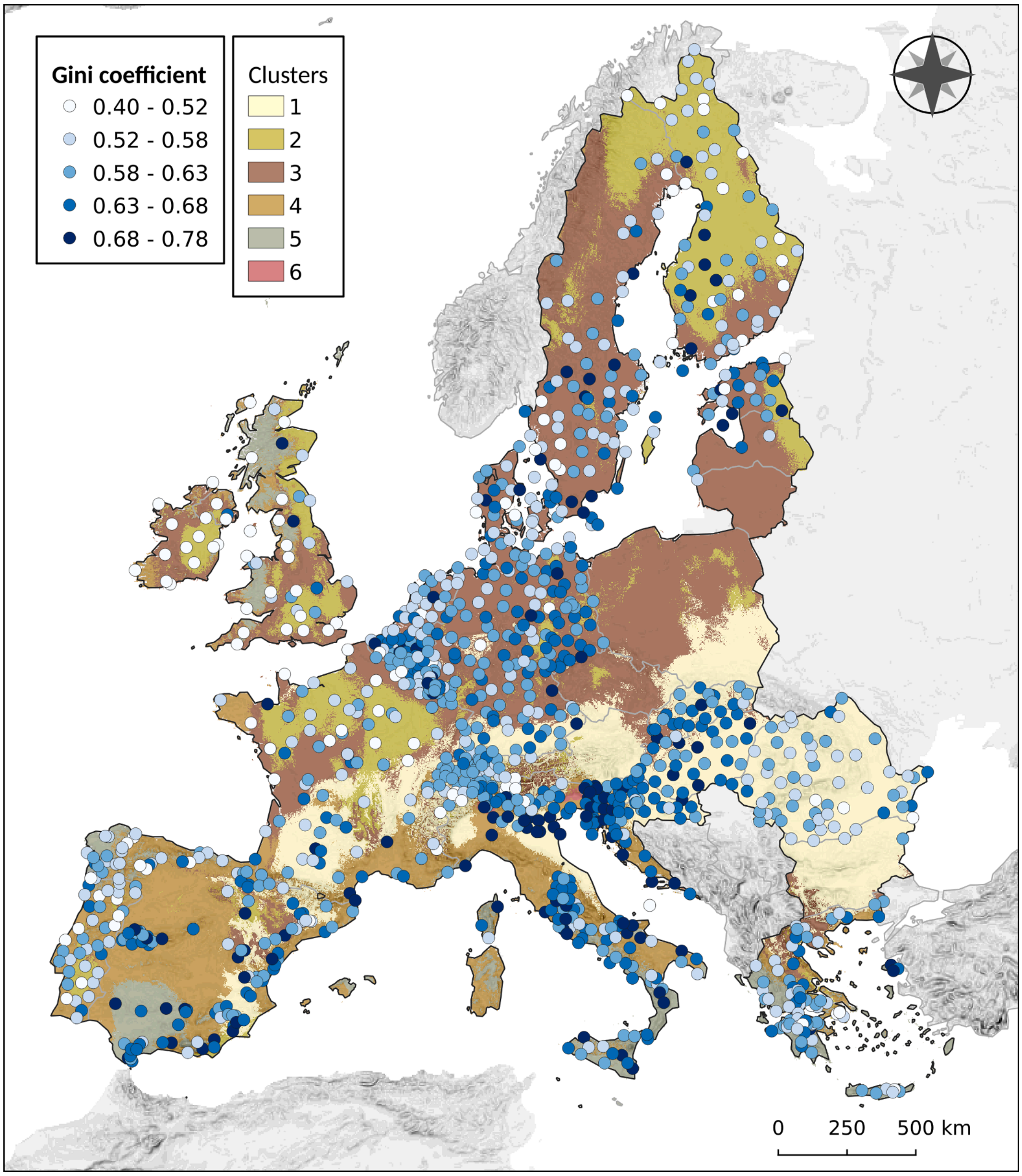

Fig. 2. Gini coefficients (G) for the 1181 stations across Europe using all rainfall erosive events included in the REDES database. As a background map, the six K-means clusters as defined by Ballabio et al. (2017) are shown.

2016; Signorell, 2020). As stated by Rajaram et al. (2017) it cannot be used to compare diversity distributions that have different levels of scale. Jost (2006) concluded that H is not a poor coefficient of diversity; on the contrary, it is the most profound and useful of all diversity indices, but its value gives the uncertainty rather than the diversity. If H is chosen as a diversity coefficient, then all communities that share a particular value of H are equivalent with respect to their diversity (according to this coefficient). As such, it is an adequate measure for estimating diversity in annual rainfall erosivity among gauging stations in Europe. As indicated by Mishra et al. (2009), the maximum value of H is obtained if all rainfall erosivity values have the same probability of occurrence. On the other hand, a value of H close to zero is obtained in case that probability of single rainfall erosivity value is close to 1 and for all others close to 0 (Mishra et al., 2009). As noted by Mishra et al. (2009), in such a case one has a complete information about the state the system is in. Thus, H indicates our uncertainty about the rainfall erosivity state (Mishra et al., 2009).

The Lorenz asymmetry coefficient (LA) is also used in this study because different shapes of the Lorenz curve can yield the same G value and thus asymmetry coefficient can be regarded as a supplement coefficient (Damgaard and Weiner, 2000; Masaki et al., 2014):

$$LA = F + L \tag{4}$$

$$F = \frac{m + \delta}{n} \tag{5}$$

$$L = \frac{\sum_{i=1}^{m} q_i + \delta q_{m+1}}{\sum_{i=1}^{n} q_i} \tag{6}$$

$$\delta = \frac{\overline{Q} - q_m}{q_{m+1} - q_m} \tag{7}$$

where m is the number of rainfall erosivity events with a value less than mean rainfall erosivity ($\overline{Q}$), n is the sample size, q_i is sorted rainfall erosivity data used to plot the Lorenz curve (Damgaard and Weiner, 2000; Masaki et al., 2014). With the introduction of the LA two Lorenz

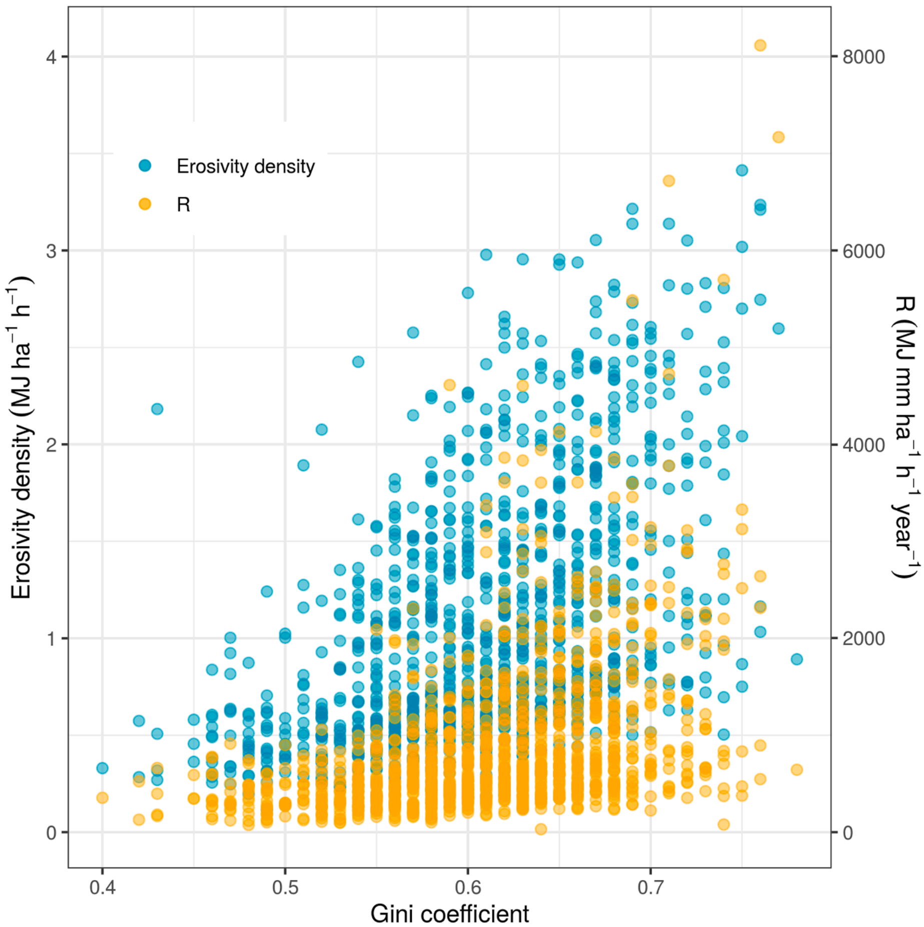

Fig. 3. Relationship between calculated Gini coefficients (G) and corresponding annual rainfall erosivity (R) and erosivity density (R/P) for the investigated 1181 stations.

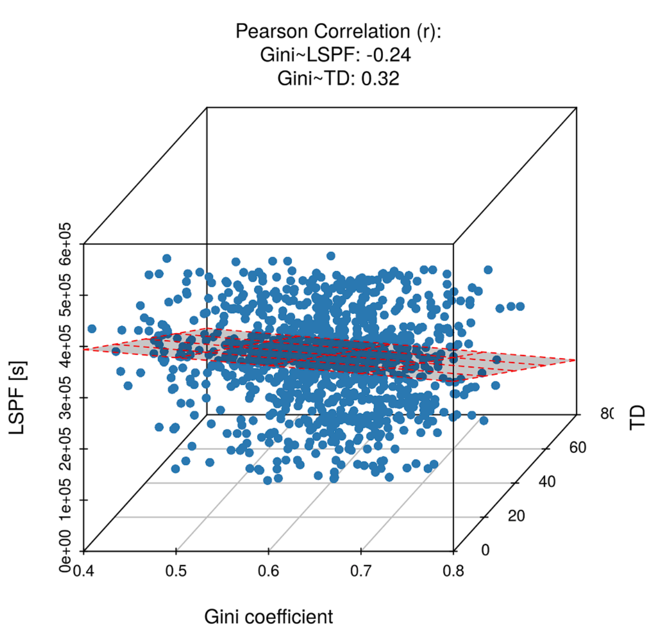

Fig. 4. Relationship between calculated Gini coefficient (G) and annual number of thunderstorm days (TD) and large-scale precipitation fraction (LSPF) for the investigated 1181 stations. The values shown in the header are Pearson correlation coefficients and the surface is a regression plane for linear regression LSPF ~ G + TD.

curves with identical G value can be distinguishable in terms of their asymmetry. More specifically, there is a difference if LA is larger or smaller than 1, while a value of 1 indicates a symmetric Lorenz curve. When analyzing future changes in flow regimes Masaki et al. (2014) interpreted LA coefficient as follows: when LA $>$ 1, the inequality is mostly due to a small number of very large river discharges; whereas LA $<$ 1, the inequality is due to a large number of very small discharges. In our study on rainfall erosive events, LA $>$ 1 means that the inequality can be attributed to a small number of high erosive rainfall events while in the case when LA $<$ 1, the inequality is due to a large number of low erosive rainfall events. One must bear in mind that rainfall erosive events can be quite intermittent when compared to flow discharges in rivers that is often a more continuous process.

As an illustrative example, in order to have a better understanding of above described coefficients, a hypothetical case of ten different erosive events is presented (Table 2). Thus, in all six presented cases, the total erosivity of these ten events is 1000 MJ mm ha^{-1}h^{-1}. The main difference between the presented cases is the temporal distribution of the rainfall erosivity between the events. Therefore, in some cases events are similar to each other, while in other cases some events are much larger than others.

All the calculations are performed using R software and using ‘REAT’, ‘ineq’ and ‘DescTools’ packages (Signorell, 2020; Wieland, 2019; Zeileis and Kleiber, 2014). All erosive rainstorms (more than 300,000) included in the REDES database are used in the calculation of the above-mentioned coefficients. Thus, for every station, all available data is used to construct the Lorenz curve and calculate above mentioned metrics.

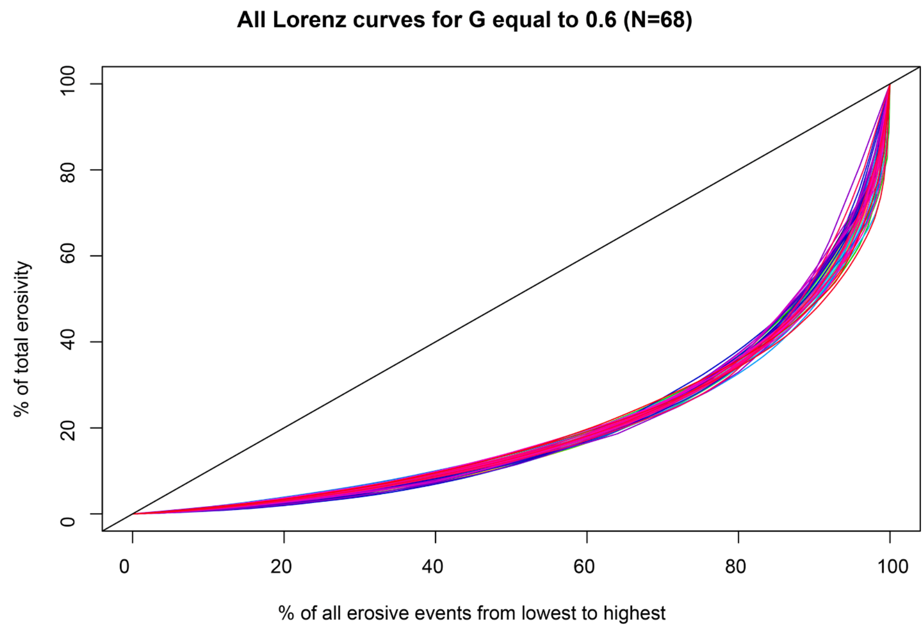

Fig. 5. Possible distribution of the Lorenz curves for the same value of the Gini coefficient (G). Every colored line indicates data from one station out of 68 presented that have a G value equal to 0.6.

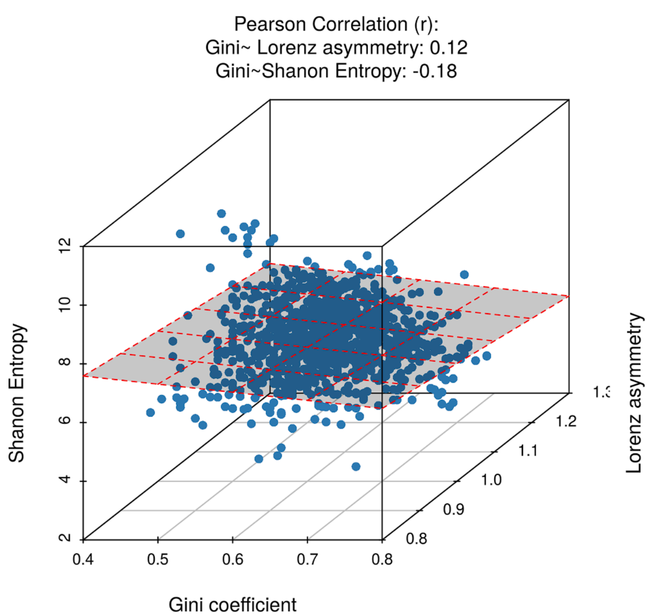

Fig. 6. Relationship between Gini coefficient (G) and Lorenz asymmetry coefficient (LA) and Shannon entropy (H) for the investigated 1181 stations. The values shown in the header are Pearson correlation coefficients and the surface is a regression plane for linear regression H ~ G + LA.

2.3. Threshold values and seasonality characteristics

The threshold values used in this study are important for better understanding of the Lorenz curve and rainfall erosivity characteristics across Europe. Therefore, the focus is also on the erosivity threshold value that is indicated in Fig. 1 and labelled as D50, and on the corresponding rainfall erosivity value R50. The D50 shows the percentage of rainfall erosive events that contribute to the 50% of the total erosivity (the x-axis on Fig. 1 corresponding to the 50% of the y-axis), while the R50 can be defined as the weighted median value. This is the rainfall erosivity event x_k that satisfies next two conditions:

$$\sum_{i=1}^{k-1} w_i < 1/2 \text{and} \sum_{i=k+1}^{n} w_i < 1/2 \tag{8}$$

where n is sample size (i.e. number of rainfall erosive events per station), w_i are rainfall erosivity values of ordered sample. Consequently, the D50 is the position (i.e. rank) of the rainfall erosivity event x_k in sorted sample of all rainfall erosive events:

$$D50 = (x_k/n)^*100 \tag{9}$$

Comparing the station Moor House (UK-1509) with the station Overkalix-Svartbyn (SE1390), in the first case (UK-1509) around 97% of all events contribute to the 50% of the total erosivity while only 3% of the (more extreme rainfall) events contribute to the other half of the total erosivity. In the second case (SE-1390), the D50 threshold value is around 19%. Thus, the differences among the rainfall erosive events are not as large as in the case of the first station. Moreover, this D50 threshold value is also connected to a specific rainfall erosivity value (R50). Thus, the R50 is the actual value of the erosive rainfall event as can also be seen from Fig. 1.

Furthermore, the seasonality of the most extreme events (i.e. events larger than R50 threshold) in comparison to seasonality of all rainfall erosive events is also investigated with aim to enhance knowledge about rainfall erosivity. Thus, mean monthly occurrence (μ_{50}) of the most extreme events (larger than R50 threshold) and standard deviation (σ_{50}) of these events (given in months) are analyzed in comparison to all rainfall erosive events (μ_{ALL} and σ_{ALL}). Therefore, next definitions are used:

$$\mu_{50} = \sum S_{50}/n_{50} \text{ and } \mu_{ALL} = \sum S_{ALL}/n \tag{10}$$

$$\sigma_{50} = \sqrt{\sum (S_{50} - \mu_{50})^2/(n_{50} - 1)} \text{ and } \sigma_{ALL} = \sqrt{\sum (S_{ALL} - \mu_{ALL})^2/(n-1)} \tag{11}$$

where S_{50} and S_{ALL} are months (i.e. numeric values; Jan-1, Feb-2, etc.) in which erosive events occurred for the events larger than the R50 threshold and all erosive events, respectively. Moreover, n_{50} is number of events above the R50 threshold. Similar concept is frequently used when investigating seasonal occurrence of floods where flood dates are

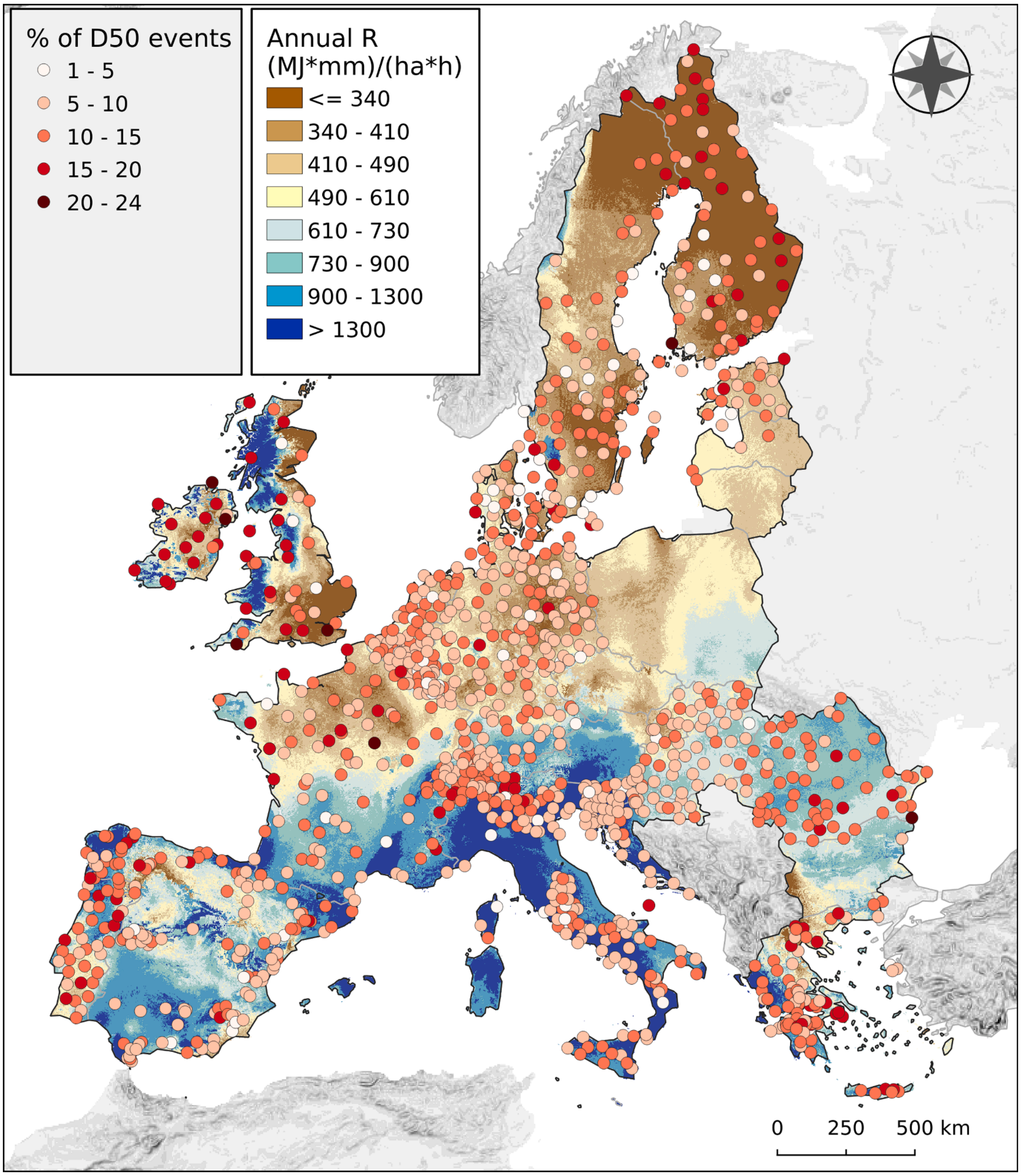

Fig. 7. Percentage of rainfall erosive events by number that contribute to the 50% of the total erosivity (D50). Rainfall erosivity map of Europe is shown as background (Panagos et al., 2015a).

represented by numeric values (Bezak et al., 2015a; Burn, 1997). For example, let's assume that a station with annual erosivity of 140 MJ mm $ha^{-1}h^{-1}$ has 5 rainfall erosive events during a year: 2 events with 10 MJ mm $ha^{-1}h^{-1}$ each that occurred in May, 2 events with 25 MJ mm $ha^{-1}h^{-1}$ each that occurred in July and October and 1 event with 70 MJ mm $ha^{-1}h^{-1}$ that occurred in August. In this hypothetical example, the largest event contributes to the 50% of the total erosivity and other four events to the other 50%. Therefore, the R50 value as defined in Eq. (8) (as weighted median) in this case equals to 25 MJ mm $ha^{-1}h^{-1}$. Additionally, it can be seen that the mean month occurrence of the event larger than the R50 (μ_{50}) is August (i.e. 8). While the mean month occurrence of all rainfall erosive events is July (μ_{ALL} equals 7). Furthermore, the standard deviation of the occurrence of all rainfall erosive events is 2.1 (σ_{ALL}), while in this example the standard deviation of only one event larger than R50 cannot be computed (σ_{50}). The idea behind calculating μ_{50}, σ_{50}, μ_{ALL} and σ_{ALL} is to investigate seasonal characteristics of the most erosive rainfall events (larger than R50) and if these are different than characteristics of all rainfall erosive events (i.e. including less erosive rainfall events). It should be noted that μ_{50} and σ_{50} should be analyzed simultaneously in order to obtain information about the actual seasonal characteristics of the rainfall erosivity.

3. Results and discussion

3.1. Erosivity characteristics in Europe through Lorenz curve characteristics and Shannon entropy

Table 3 provides an overview of the derived Lorenz curves and calculated Gini coefficient (G), normalized Gini coefficient (G*), Lorenz asymmetry coefficient (LA), and Shannon entropy (H) for all 1181 stations included in the REDES database. These coefficients are selected to describe the inequality (G and G* and LA as a supplement coefficient to the G and G*) and diversity (H) of the rainstorms erosivity in Europe. Some descriptive statistics of these metrics for the six K-means clusters defined after Ballabio et al. (2017) are reported in Table 4. From the information reported in Table 4, one can notice that there is no big

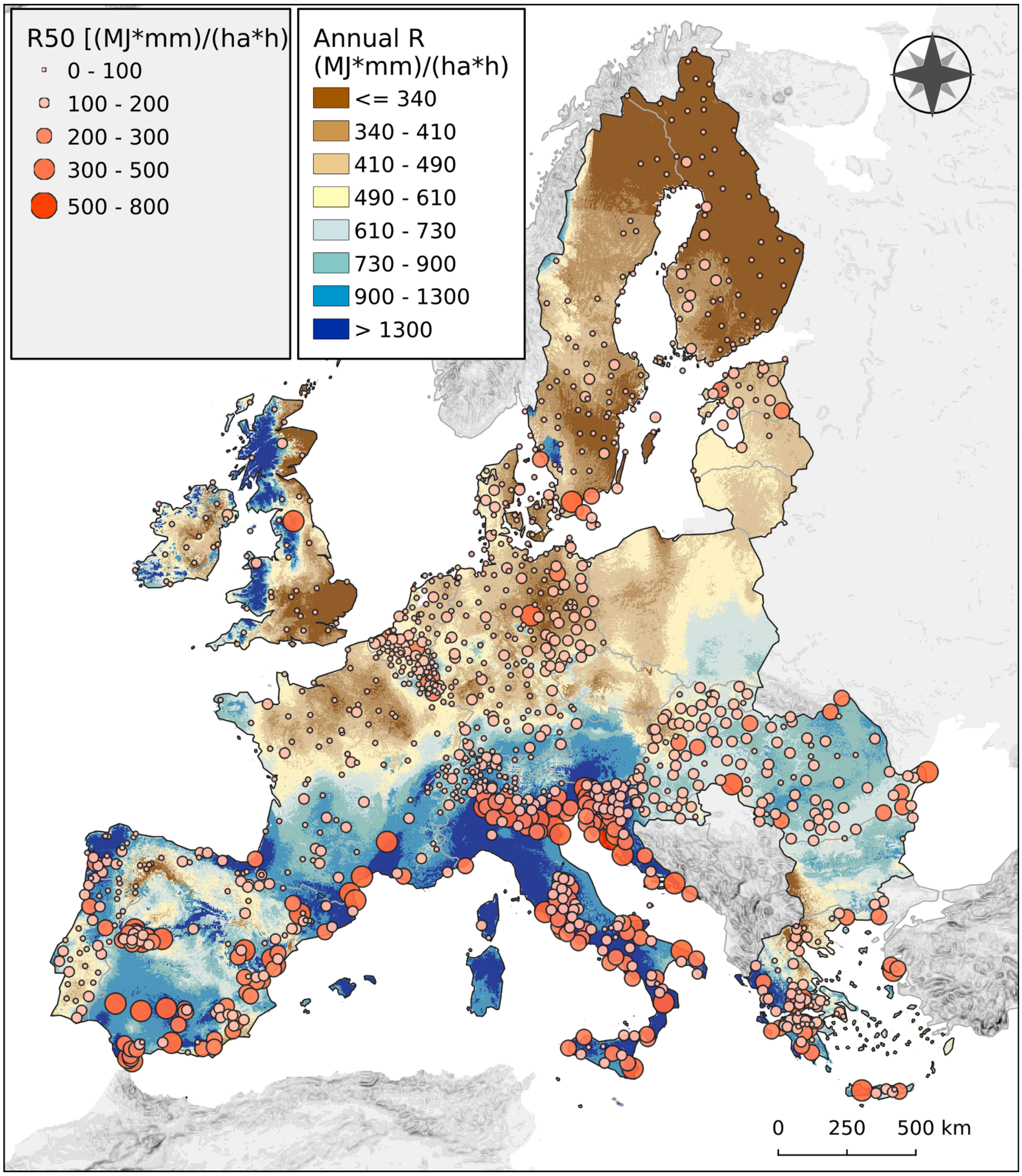

Fig. 8. Events larger than R50 threshold value contribute to the 50% of the total erosivity. Annual rainfall erosivity map is shown as background.

differences in reported G, H and LA values among the six K-means clusters. The Alpine region, defined by the K-means cluster 6, shows the highest erosivity in Europe and a significant difference compared to the K-means clusters 5; in terms of seasonality and erosivity values. In this regard, it is worth to mention that K-means cluster 6 is also the cluster with the lowest number of stations. Highest mean G and H values are both observable in K-mean cluster 6, which suggest a large diversity (inequality) in the rainstorm erosivity values. A situation represented by the presence of a variable set of small and large erosive rainfall events, with a large number of relatively small erosive rainfall events (i.e. small from the perspective of the Alpine region) according to the mean LA value that is smaller than 1 can be seen according to the Table 4. Furthermore, stations located in cluster 6 are the ones with the lowest LA value in Europe (Tables 3 and 4).

In Europe, G ranges from 0.4 to 0.78 with a mean value of 0.61 (Table 3). While no significant differences can be observed between the K-means clusters Table 3, some geographical patterns can be detected in Fig. 2 reporting the G values computed for each station. Slightly higher G values (average value 0.61) are characteristic of the Mediterranean region, which is mostly spatially described by K-means clusters 4 and 5 (i.e. Italy, Greece, Croatia, parts of Spain, Slovenia). Lower G values compared to the mean EU (0.61) are found in parts of France, United Kingdom and Scandinavia, which are mostly part of the K-means clusters 2 and 3 (Fig. 2). These areas have in most cases smaller rainfall erosivity compared to the Mediterranean region. Similar to the G values, the H value is above the EU average (6.44) in K-means clusters 4, 5 and 6 (including 1), and below-average in the K-means clusters 2 and 3 (Tables 3 and 4). In case of the LA values, an opposite spatial trend can be observed, with values slightly above the EU average calculated for K-means clusters 2 and 3 (Tables 3 and 4). The LA values equal or higher than 1 are found in around 75% of all stations (Table 3). Conclusively, the inequality inferable from the combined analysis of G, H and LA can mostly be attributed to a small number of high erosive rainfall events, rather than to a large number of low erosive events (e.g., K-means cluster 6). Furthermore, it should be noted these low and high erosive rainfall events are site-specific, which means that, for example, a low erosive rainfall event in the Mediterranean area can be regarded as a high erosive rainfall event in northern part of Europe.

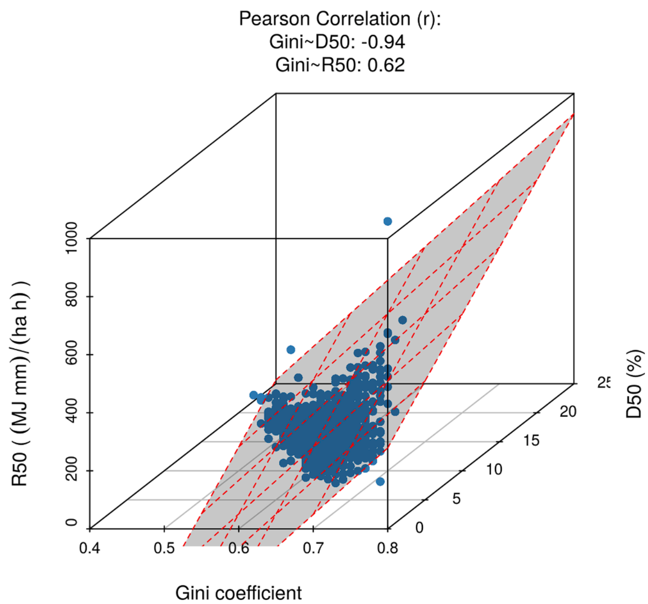

Fig. 9. Relationship between the D50, R50 and Gini coefficient (G). The values shown in the header are Pearson correlation coefficients and the surface is a regression plane for linear regression R50 ~ G + D50.

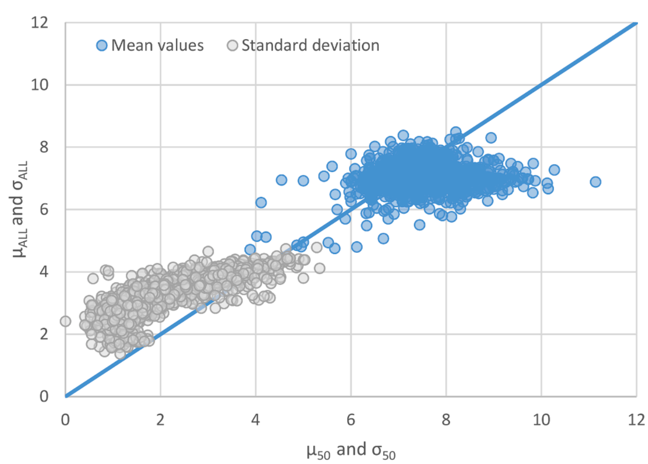

Fig. 10. Relationship between the seasonal characteristics of the most erosive rainfall events and all rainfall erosive events (μ_{50}, σ_{50}, μ_{ALL} and σ_{ALL}).

Regarding the spatial trend, G tends to slightly decrease with increasing latitude (i.e. 0.02 G per 10° according to the best-fitted linear trend line). By contrast, no evident relationship with longitude is found. The same is true for the H that decreases with increasing latitude (i.e. 0.3H per 10° according to the best-fitted linear trend line) (Fig. S1). On the other hand, the LA increases with increasing latitude (i.e. 0.03 LA per 10° according to the best-fitted linear trend line) (Fig. S2). Thus, it emerges that in the northern part of Europe there is generally a smaller number of highly erosive rainfall events (i.e. LA larger than 1). Moreover, here the temporal distribution of erosive events appear more equal distributed, as highlighted by the G and H values compared to the southern part of Europe (Fig. 2). Although, as already noted the detected differences are not highly significant.

Additionally, the relationship between the calculated G, LA and H and annual rainfall erosivity (R) is also investigated (Fig. 3). Thus, it can be seen that, as expected, higher G values are associated with higher R-factor values. Thus, only few events are contributing to the larger percent of erosivity (>90%), which can also be confirmed by the LA values shown in Tables 3 and 4. The dependence between G and R is stronger when only stations with R values larger than 1000 MJ mm ha^{-1}h^{-1} yr^{-1} are considered, compared to the case when all stations are taken into consideration (Fig. 3). In case of stations with R smaller than 1000 MJ mm ha^{-1}h^{-1} yr^{-1}, G values range from ca. 0.4 to 0.8 (Fig. 3). A similar relationship can also be seen comparing H and R values (Fig. S3). On the other hand, the LA slightly decreases with increasing annual rainfall erosivity (0.02 LA per 1000 MJ mm ha^{-1}h^{-1} yr^{-1} according to the best-fitted linear trend line) (Fig. S4). Additionally, stations with smaller R (i.e. less than 1000 MJ mm ha^{-1}h^{-1} yr^{-1}) can have LA in the range between 0.8 and 1.2. It can also be seen that G values are related to the erosivity density (Fig. 3) defined as the ratio between R and mean annual precipitation (P) (Diodato et al., 2019; Panagos et al., 2016a, 2015a). Highest values of the erosivity density can be found in the Mediterranean area (Italy, Croatia, Slovenia, parts of Spain and Greece) (Panagos et al., 2015a). These areas also characterized by larger G values. Lower G values are associated with areas with lower erosivity density. It should be noted that through the use of G, H and LA one can captures the temporal variability in rainfall erosivity.

Furthermore, Bezak et al. (2021a) proposed atmospheric drivers (e.g. thunderstorm days, large-scale precipitation fraction) of rainfall erosivity and here we analyse their relationship to G. It can be seen that G slightly increases with annual number of thunderstorm days (TD) (Enno et al., 2020) and slightly decreases with increasing large-scale precipitation fraction (LSPF) (Fig. 4). Similar relationship can also be detected among H and two mentioned atmospheric variables, while opposite relationship is found for the LA. However, it should be noted that correlation in the above mentioned cases is weak. Furthermore, we also found an even weaker relationship between G and other tested variables such as CAPE and CP (Section 2.1). It clearly emerges that G is slightly higher in areas with more frequent thunderstorms (i.e. Mediterranean area) and slightly lower in areas where large scale frontal systems have larger effect in precipitation generation. Moreover, no significant relationship is found between the G and the erosivity synchrony scale (Rsync) as calculated by Bezak et al. (2021a).

As already indicated different shapes of the Lorenz curve can be characterized by the same or similar G value (Fig. 5). Thus, here we present a sample of 68 different stations with very similar values of G (i.e. G of 0.6) despite the fact that Lorenz curve for these stations are not identical (Fig. 5). Therefore, the LA can provide additional information, as it is shown in the above paragraphs. Quite interestingly, there is no clear relationship between G and LA (see scattered cloud in Fig. 6). Thus, LA values above 1 and values below 1 (i.e. large number of less erosive rainfall events) can occur at stations with low or high G (Fig. 6). Only a slight decreasing trend for H with increasing G can be observed (R^2 = 0.05). The H considers richness (number of rainfall erosive events with different erosivity) and evenness (occurrence probability of rainfall erosive events with different erosivity) at the same time. H can be decreasing due to the former or latter characteristic (low richness or low evenness). To understand what is the cause of lower H in case of higher G, one should understand that higher G means lower evenness. The H is namely at its maximum when all rainfall erosive events with different erosivity (potentially high richness) are equally likely (G would be zero). The value of H is then only a function of richness. The main cause for decreasing H for increasing G is decreasing evenness of rainfall erosive events. The increasing G should possibly lower H to a larger extent as seen in Fig. 6 and could partially be counter-balanced by a higher richness at higher G.

3.2. Erosivity threshold values and seasonal characteristics

The results of the two threshold value indicators D50 and R50 used to capture the severity of rainfall erosivity across Europe are shown in this section (Figs. 7 and 8). D50 expresses the percentage of rainfall erosive events that contribute to 50% of the total erosivity. The observed values range from 1 to 24%, with a mean value of 11%. It means that on average ca. 90% of the rainfall events account only for ca. 50% of the

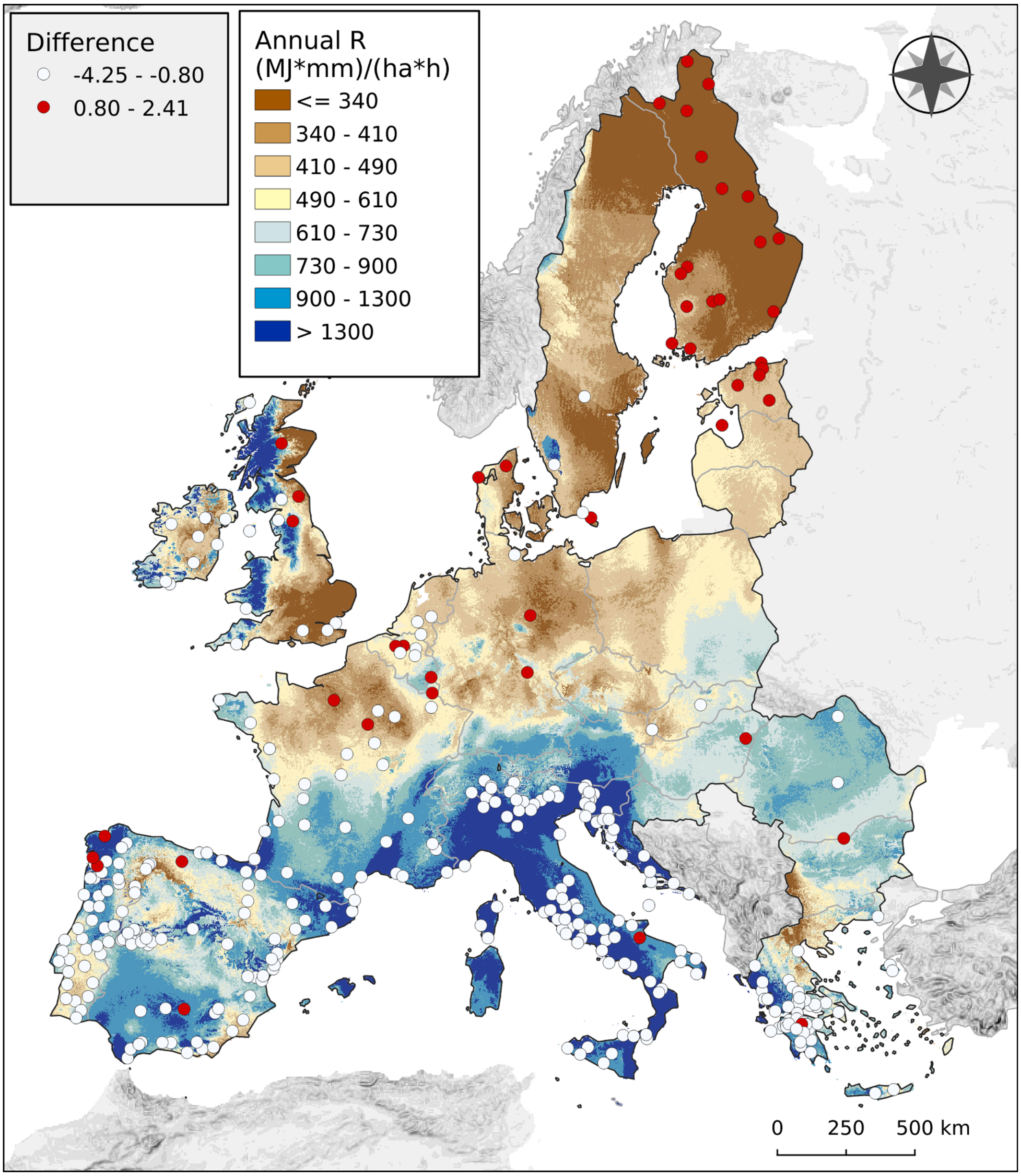

Fig. 11. Difference in the mean month occurrence (μ_{ALL}- μ_{50}). Mean differences smaller than 0.8 months are not shown. Negative values indicate that that most erosive rainfall events (i.e. larger than R50, μ_{50}), on average, occur later in the year than less erosive events (μ_{ALL}). Positive values indicate opposite situation.

total erosivity (Fig. 7). In extreme cases, ca. 50% of the total erosivity can be attributed to only one or two very severe events (i.e. white dots shown in Fig. 7). Spatial patterns shown in Fig. 7 are similar to the ones shown in Fig. 2. Moreover, González-Hidalgo et al. (2009) showed that 50% of the eroded soil were produced by 10% of total daily erosive events. The R50 is the weighted median value of all erosive events and ranges from 19 to 979 MJ mm ha^{-1}h^{-1}, with a mean value of 119 MJ mm ha^{-1}h^{-1}. Additionally, if one looks at the R50 it can be seen that this threshold values are more correlated to the R-factor ($R^2 = 0.45$). Thus, rainfall erosive events larger than this threshold contribute to the 50% of the total annual rainfall erosivity. The largest R50 values in Europe are characteristic of areas with the highest rainfall erosivity, e.g., Slovenia and Italy. On the other hand, lower R50 values are characteristic of Scandinavia and central Europe, which are generally characterized by rather lower R values.

Furthermore, the relationship between the D50 and R50 thresholds and the G is analyzed. This can be seen on Fig. 9 showing how the D50 threshold is well correlated to G ($R^2 = 0.87$) (compare also the results on Figs. 7 and 2). This can be regarded as an expected result since D50 values are calculated based on the Lorenz curve characteristics (Fig. 1). The scatter observed on Fig. 9 is related to variability of the LA for a fixed G (see Fig. 6). R50 has a lower correlation with the G with a large scatter at higher values of G (Fig. 9). In case of R50 and G, the Pearson correlation coefficient is a bit lower ($R^2 = 0.47$) compared to the D50-G correlation.

The seasonal characteristics of the most erosive rainfall events are investigated by comparing the μ_{50} and σ_{50} to μ_{ALL} and σ_{ALL} coefficients. In case of the seasonal characteristics (i.e. μ_{50} vs. μ_{ALL}), it can be observed that highest erosive rainfall events (i.e. larger than R50) are more shifted towards autumn (Fig. 10). While the mean value of μ_{ALL} is July (i.e. a value of 7), the mean value of μ_{50} is mid-July (i.e. 7.4) (Fig. 10). However, the scatter among stations is larger in case of the most erosive rainfall events as compared to all rainfall erosive events (Fig. 10). An alternative way to present the map of the differences in the mean month occurrence (μ_{ALL}- μ_{50}) ignoring differences smaller than 0.8 months. It can be seen that for most stations the highest erosive

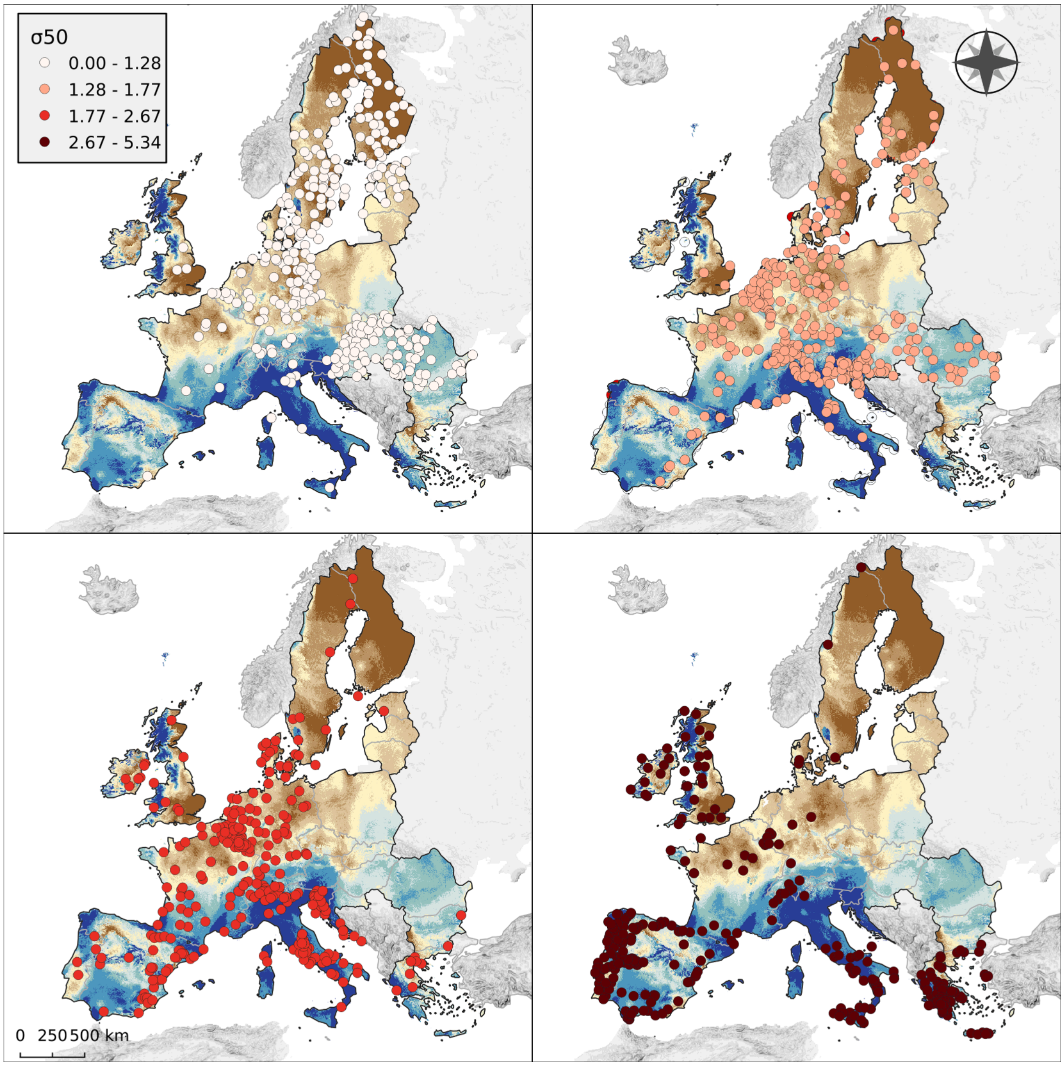

Fig. 12. Standard deviation σ_{50} is shown. Four different groups of σ_{50} values are presented while for each group a separate plot is shown in order to identify differences among groups.

rainfall events (μ_{50}) occur later in the year (Fig. 11). This is especially evident in case of the Mediterranean area. As indicated by Ballabio et al. (2017) the erosivity in this area is very high in the period starting from early summer to late autumn. The main mechanism could be higher potential for the occurrence of the convective precipitation, which is clearly related to the rainfall erosivity (Bezak et al., 2021a). Moreover, relatively high number of less-erosive events also occur in spring compared to summer (Fernandez-Raga et al., 2017), which could yield differences shown in Fig. 11. Additionally, the variability in the occurrence of all rainfall erosive events and the most extreme ones (σ_{ALL} and σ_{50}) is investigated (Figs. 10 and 12). It can be seen that the variability of most erosive rainfall events (σ_{50}) decreases in the direction from south-west to north-east (Fig. 12). Thus, in the north-eastern part of EU the most erosive rainfall events are the most localized (i.e. smaller standard deviation) and are occurring mostly in summer (Ballabio et al., 2017). On the other hand, this variability is the largest in the Mediterranean area and British Isles (Fig. 12). Furthermore, it can also be seen that the range of σ_{50} is larger than the range of σ_{ALL} (Fig. 10). It should be noted that extreme erosive rainfall events are not the only drivers of the soil erosion processes and that other factors such as topography, soil characteristics, or vegetation cover also affect soil erosion rates. It should be noted that in autumn vegetation phenology is different compared to summer and less rainfall is intercepted by vegetation in leafless periods (e.g., Zabret et al., 2018) and this has an important effect on the soil erosion. A shift of extreme erosive rainfall events with high erosivity towards months in a year with less vegetation cover may have large implication for high soil erosion rates at such sites.

3.3. Limitations of the study

The analysis here presented has a few limitations that need to be mentioned. First, it should be noted that due to the mentioned scarcity of data, the pluviographic records forming the REDES database cover different periods and, in some cases, the length of the records can differ substantially. More precisely, a few stations (i.e. less than 3–5%) have only about 5 years data available, which in some cases could not be enough to adequately capture the entire variability of rainstorm erosivity. However, it should be noted that a lot of stations with limited amount of data are located in the Mediterranean region and with relatively large number of events. For example, there are 5 stations with 3 years of data but all these stations have more than 60 erosive rainfall events in this 3 years (i.e. more than 20 per year). These relatively short data periods have some effect on the derived Lorenz curves and derived coefficients. A sensitivity investigation using selected stations shows that using 50% of the station-data included in the REDES yields differences up to 10–15% in the calculated coefficients. Nevertheless, the REDES database is the most complete database at the time being available on ground-measured rainfall amounts from which actual rainfall intensity can be computed for a large number of points across Europe. As such, it is worth using it to gain insights on large-scale spatiotemporal variability of rainfall erosivity.

4. Conclusions

This study investigates temporal and seasonal characteristics of the rainfall erosive events in Europe using the Lorenz curve and a large set of derived indices, i.e. Gini coefficient (G), normalized Gini coefficient (G*), Lorenz asymmetry coefficient (LA), Shannon entropy (H) coefficient and D50 and R50 thresholds. More than 300,000 rainfall erosive events from 1181 REDES rainfall gauging stations is used in this analysis.

The observed temporal distribution of the rainfall erosive events in the Europe has high variability. The G ranges from 0.4 to 0.8, with a mean value of 0.61 (SD 0.06). Among the six K-means clusters defined for Europe, relatively small differences in the mean G, H and LA values are observed. The most distinct differences are observed in the K-means cluster that covers the Alpine region, which also shows the highest R values. G slightly decreases from south to north of Europe. The same relationship is found for H, while opposite spatial trends are noted for LA. It is observed that G increases with increasing R, although the dependence is not as strong as one would have expected. In Europe, the H ranges between 4 and 10 and is only slightly decreasing with increasing G and R. Furthermore, G also increases with erosivity density and annual number of thunderstorm days (TD), while it slightly decreases with large-scale precipitation fraction (LSPF). Although it should be noted that the G correlation with atmospheric variables is rather weak or even very weak.

The mean value of the D50 threshold in Europe is 11% (ranging from 1 to 24%), which means that, on average, 11% of all rainfall erosive events contribute to the 50% of the total erosivity while around 90% of events contribute the other half. The spatial pattern of the D50 is similar to the pattern determined by G. Moreover, R50 also varies across Europe where the largest values can be detected in the Mediterranean and Alpine areas.

In the majority of the stations, seasonal characteristics the most erosive rainfall events (μ_{50} and σ_{50}) are not the same as seasonal characteristics of the entire series of rainfall erosive events (μ_{ALL} and σ_{ALL}). Thus, the majority of higher rainfall erosive events (i.e. larger than R50) is slightly shifted to the autumn (i.e. $\mu_{50} > \mu_{ALL}$). Differences in the mean month occurrence (μ_{ALL}- μ_{50}) are the largest in the Mediterranean area where extreme erosive rainfall events can occur in summer and in autumn while in other parts of Europe the extreme erosive rainfall events are more localized in the summer. This is also confirmed by the variability (σ_{50}) of the most erosive rainfall events that decreases from south-west to north-east of Europe ($\sigma_{50} > \sigma_{ALL}$).

The presented results can be regarded as a new important piece in the mosaic of spatiotemporal rainfall erosivity variability in Europe. From the analysis it clearly emerged that regional temporal rainfall erosivity patterns are not homogenous (i.e. relatively large differences among neighboring stations can be seen in Fig. 2), thus, as one could expect, local climatological conditions determine the local temporal rainfall erosivity distribution. Thus, for example, a station located in the Mediterranean area or in British Isles can have very similar temporal distribution of rainfall erosive events while of course the absolute rainfall erosivity values can be quite different. This finding can be connected to the results presented by Bezak et al. (2021a), who found that rainfall erosivity synchrony scale is generally smaller than computed precipitation synchrony scale as reported by Berghuijs et al. (2019). Moreover, the seasonal investigation reveals that the most erosive events that contribute to the 50% of the total erosivity (between 1 and 24% of all events, on average 11% of events) generally occur later in the year than less erosive events. Thus, the largest erosive events are shifted to the autumn or large number of less erosive events occur in spring. Additionally, there are relatively large differences in the seasonal variability of these events across Europe. These findings can be regarded as an important input for the soil erosion predictions from the perspective of the large-scale, process and event-based soil erosion modelling, which would allow to make a more dynamic soil erosion assessment. However, further studies are needed in order to analyze the relationship between the micro-climate drivers (e.g., Bezak et al., 2021a) and weather phenomena such as North Atlantic Oscillation (NAO) (e.g., Angulo-Martínez and Beguería, 2012; Luković et al., 2015) and rainfall erosivity at large spatial scales, which could help with the forecast of the most erosive rainfall events that are one of the factors affecting soil erosion rates.

Declaration of Competing Interest

The authors declare that they have no known competing financial interests or personal relationships that could have appeared to influence the work reported in this paper.

Acknowledgements

N. Bezak and M. Mikoš kindly acknowledge the financial support from the Slovenian Research Agency (research core funding No. P2-0180). P. Borrelli is funded by the EcoSSSoil Project, Korea Environmental Industry & Technology Institute (KEITI), Korea (Grant No. 2019002820004). The critical and useful comments made by four anonymous reviewers and associate editor greatly improved this work.

Appendix A. Supplementary material

Supplementary data to this article can be found online at https://doi.org/10.1016/j.catena.2021.105577.

References

Almagro, A., Oliveira, P.T.S., Nearing, M.A., Hagemann, S., 2017. Projected climate change impacts in rainfall erosivity over Brazil. Sci. Rep. 7 https://doi.org/10.1038/s41598-017-08298-y.

Angulo-Martínez, M., Beguería, S., 2012. Trends in rainfall erosivity in NE Spain at annual, seasonal and daily scales. Hydrol. Earth Syst. Sci. 16, 3551–3559. https://doi.org/10.5194/hess-16-3551-2012.

Bagarello, V., Di Stefano, C., Ferro, V., Pampalone, V., 2011. Using plot soil loss distribution for soil conservation design. Catena 86, 172–177. https://doi.org/10.1016/j.catena.2011.03.009.

Ballabio, C., Borrelli, P., Spinoni, J., Meusburger, K., Michaelides, S., Beguería, S., Klik, A., Petan, S., Janeček, M., Olsen, P., Aalto, J., Lakatos, M., Rymszewicz, A., Dumitrescu, A., Tadić, M.P., Diodato, N., Kostalova, J., Rousseva, S., Banasik, K., Alewell, C., Panagos, P., 2017. Mapping monthly rainfall erosivity in Europe. Sci. Total Environ. 579, 1298–1315. https://doi.org/10.1016/J.SCITOTENV.2016.11.123.

Beguería, S., Serrano-Notivoli, R., Tomas-Burguera, M., 2018. Computation of rainfall erosivity from daily precipitation amounts. Sci. Total Environ. 637–638, 359–373. https://doi.org/10.1016/j.scitotenv.2018.04.400.

Berghuijs, W.R., Allen, S.T., Harrigan, S., Kirchner, J.W., 2019. Growing Spatial Scales of Synchronous River Flooding in Europe. Geophys. Res. Lett. 46, 1423–1428. https://doi.org/10.1029/2018GL081883.

Bezak, N., Ballabio, C., Mikoš, M., Petan, S., Borrelli, P., Panagos, P., 2020. Reconstruction of past rainfall erosivity and trend detection based on the REDES database and reanalysis rainfall. J. Hydrol. 590, 125372 https://doi.org/10.1016/j.jhydrol.2020.125372.

Bezak, N., Borrelli, P., Panagos, P., 2021a. A first assessment of rainfall erosivity synchrony scale at pan-European scale. Catena 198, 105060. https://doi.org/10.1016/j.catena.2020.105060.

Bezak, N., Horvat, A., Šraj, M., 2015a. Analysis of flood events in Slovenian streams. J. Hydrol. Hydromechanics 63. https://doi.org/10.1515/johh-2015-0014.

Bezak, N., Mikoš, M., Borrelli, P., Alewell, C., Alvarez, P., Anache, J.A.A., Baartman, J., Ballabio, C., Biddoccu, M., Cerdà, A., Chalise, D., Chen, S., Chen, W., De Girolamo, A. M., Gessesse, G.D., Deumlich, D., Diodato, N., Efthimiou, N., Erpul, G., Fiener, P., Freppaz, M., Gentile, F., Gericke, A., Haregeweyn, N., Hu, B., Jeanneau, A., Kaffas, K., Kiani-Harchegani, M., Villuendas, I.L., Li, C., Lombardo, L., López-Vicente, M., Lucas-Borja, M.E., Maerker, M., Miao, C., Modugno, S., Möller, M., Naipal, V., Nearing, M., Owusu, S., Panday, D., Patault, E., Patriche, C.V., Poggio, L., Portes, R., Quijano, L., Rahdari, M.R., Renima, M., Ricci, G.F., Rodrigo-Comino, J., Saia, S., Samani, A.N., Schillaci, C., Syrris, V., Kim, H.S., Spinola, D.N., Oliveira, P.T., Teng, H., Thapa, R., Vantas, K., Vieira, D., Yang, J.E., Yin, S., Zema, D.A., Zhao, G., Panagos, P., 2021b. Soil erosion modelling: A bibliometric analysis. Environ. Res. 197, 111087 https://doi.org/10.1016/j.envres.2021.111087.

Bezak, N., Rusjan, S., Petan, S., Sodnik, J., Mikoš, M., 2015b. Estimation of soil loss by the WATEM/SEDEM model using an automatic parameter estimation procedure. Environ. Earth Sci. 74, 5245–5261. https://doi.org/10.1007/s12665-015-4534-0.
Borrelli, P., Alewell, C., Alvarez, P., Anache, J.A.A., Baartman, J., Ballabio, C., Bezak, N., Biddoccu, M., Cerdà, A., Chalise, D., Chen, S., Chen, W., De Girolamo, A.M., Gessesse, G.D., Deumlich, D., Diodato, N., Efthimiou, N., Erpul, G., Fiener, P., Freppaz, M., Gentile, F., Gericke, A., Haregeweyn, N., Hu, B., Jeanneau, A., Kaffas, K., Kiani-Harchegani, M., Villuendas, I.L., Li, C., Lombardo, L., López-Vicente, M., Lucas-Borja, M.E., Märker, M., Matthews, F., Miao, C., Mikoš, M., Modugno, S., Möller, M., Naipal, V., Nearing, M., Owusu, S., Panday, D., Patault, E., Patriche, C.V., Poggio, L., Portes, R., Quijano, L., Rahdari, M.R., Renima, M., Ricci, G.F., Rodrigo-Comino, J., Saia, S., Samani, A.N., Schillaci, C., Syrris, V., Kim, H.S., Spinola, D.N., Oliveira, P.T., Teng, H., Thapa, R., Vantas, K., Vieira, D., Yang, J.E., Yin, S., Zema, D.A., Zhao, G., Panagos, P., 2021. Soil erosion modelling: A global review and statistical analysis. Sci. Total Environ. 146494 https://doi.org/10.1016/j.scitotenv.2021.146494.
Borrelli, P., Diodato, N., Panagos, P., 2016. Rainfall erosivity in Italy: a national scale spatio-temporal assessment. Int. J. Digit. Earth 9, 835–850. https://doi.org/10.1080/17538947.2016.1148203.
Borrelli, P., Robinson, D.A., Fleischer, L.R., Lugato, E., Ballabio, C., Alewell, C., Meusburger, K., Modugno, S., Schütt, B., Ferro, V., Montanarella, L., Panagos, P., 2017. An assessment of the global impact of 21st century land use change on soil erosion. Nat. Commun. 8 https://doi.org/10.1038/s41467-017-02142-7.
Borrelli, P., Robinson, D.A., Panagos, P., Lugato, E., Yang, J.E., Alewell, C., Wuepper, D., Montanarella, L., Ballabio, C., 2020. Land use and climate change impacts on global soil erosion by water (2015–2070). Proc. Natl. Acad. Sci. U. S. A. 117, 21994–22001. https://doi.org/10.1073/pnas.2001403117.
Burn, D.H., 1997. Catchment similarity for regional flood frequency analysis using seasonality measures. J. Hydrol. 202, 212–230. https://doi.org/10.1016/S0022-1694(97)00068-1.
Capra, A., Porto, P., La Spada, C., 2017. Long-term variation of rainfall erosivity in Calabria (Southern Italy). Theor. Appl. Climatol. 128, 141–158. https://doi.org/10.1007/s00704-015-1697-2.
Ceriani, L., Verme, P., 2012. The origins of the Gini index: Extracts from Variabilità e Mutabilità (1912) by Corrado Gini. J. Econ. Inequal. 10, 421–443. https://doi.org/10.1007/s10888-011-9188-x.
Chen, Y., Xu, M., Wang, Z., Chen, W., Lai, C., 2020. Reexamination of the Xie model and spatiotemporal variability in rainfall erosivity in mainland China from 1960 to 2018. Catena 195. https://doi.org/10.1016/j.catena.2020.104837.
Clementi, F., Gallegati, M., Gianmoena, L., Landini, S., Stiglitz, J.E., 2019. Mis-measurement of inequality: a critical reflection and new insights. J. Econ. Interact. Coord. 14, 891–921. https://doi.org/10.1007/s11403-019-00257-2.
Cowell, F.A., 2000. Measurement of inequality. In: Atkinson, A.B., Ourguignon, F. (Eds.), Handbook of Income Distribution. Elsevier, Amsterdam, pp. 87–166.
Cui, Y., Pan, C., Liu, C., Luo, M., Guo, Y., 2020. Spatiotemporal variation and tendency analysis on rainfall erosivity in the Loess Plateau of China. Hydrol. Res. 51, 1048–1062. https://doi.org/10.2166/nh.2020.030.
D'Asaro, F., D'Agostino, L., Bagarello, V., 2007. Assessing changes in rainfall erosivity in Sicily during the twentieth century. Hydrol. Process. 21, 2862–2871. https://doi.org/10.1002/hyp.6502.
Damgaard, C., Weiner, J., 2000. Describing inequality in plant size or fecundity. Ecology 81, 1139–1142. https://doi.org/10.1890/0012-9658(2000)081[1139:DIIPSO]2.0.CO;2.
Diodato, N., Borrelli, P., Panagos, P., Bellocchi, G., Bertolin, C., 2019. Communicating Hydrological Hazard-Prone Areas in Italy With Geospatial Probability Maps. Front. Environ. Sci. 7 https://doi.org/10.3389/fenvs.2019.00193.
Enno, S.-E., Sugier, J., Alber, R., Seltzer, M., 2020. Lightning flash density in Europe based on 10 years of ATDnet data. Atmos. Res. 235 https://doi.org/10.1016/j.atmosres.2019.104769.
Fernandez-Raga, M., Castro, A., Marcos, E., Palencia, C., Fraile, R., 2017. Weather types and rainfall microstructure in Leon, Spain. Int. J. Climatol. 37, 1834–1842. https://doi.org/10.1002/joc.4816.
Ferro, V., Carollo, F.G., Serio, M.A., 2020. Establishing a threshold for rainfall-induced landslides by a kinetic energy–duration relationship. Hydrol. Process. 34, 3571–3581. https://doi.org/10.1002/hyp.13821.
Gastwirth, J.L., 1971. A General Definition of the Lorenz Curve. Econometrica 39, 1037–1039. https://doi.org/10.2307/1909675.
Gini, C., 1914. On the measurement of concentration and variability of characters. Metron 63, 3–38.
González-Hidalgo, J.C., de Luis, M., Batalla, R.J., 2009. Effects of the largest daily events on total soil erosion by rainwater. An analysis of the usle database. Earth Surf. Process. Landforms 34, 2070–2077. https://doi.org/10.1002/esp.1892.
Grillakis, M.G., Polykretis, C., Alexakis, D.D., 2020. Past and projected climate change impacts on rainfall erosivity: Advancing our knowledge for the eastern Mediterranean island of Crete. Catena 193. https://doi.org/10.1016/j.catena.2020.104625.
Jawitz, J.W., Mitchell, J., 2011. Temporal inequality in catchment discharge and solute export. Water Resour. Res. 47 https://doi.org/10.1029/2010WR010197.
Jost, L., 2006. Entropy and diversity. Oikos 113, 363–375. https://doi.org/10.1111/j.2006.0030-1299.14714.x.
Kim, J., Han, H., Kim, B., Chen, H., Lee, J.-H., 2020. Use of a high-resolution-satellite-based precipitation product in mapping continental-scale rainfall erosivity: A case study of the United States. Catena 193. https://doi.org/10.1016/j.catena.2020.104602.
Lal, R., 1998. Soil erosion impact on agronomic productivity and environment quality. CRC. Crit. Rev. Plant Sci. 17, 319–464. https://doi.org/10.1016/S0735-2689(98)00363-3.
Liu, Y., Zhao, W., Liu, Y., Pereira, P., 2020. Global rainfall erosivity changes between 1980 and 2017 based on an erosivity model using daily precipitation data. Catena 194. https://doi.org/10.1016/j.catena.2020.104768.
Lorenz, M.O., 1905. Methods of measuring the concentration of wealth. Publ. Am. Stat. Assoc. 9, 209–219. https://doi.org/10.1080/15225437.1905.10503443.
Lukić, T., Basarin, B., Micić, T., Bjelajac, D., Maris, T., Marković, S.B., Pavić, D., Gavrilov, M.B., Mesaroš, M., 2018a. Rainfall erosivity and extreme precipitation in the Netherlands. Idojaras 122, 409–432. https://doi.org/10.28974/idojaras.2018.4.4.
Lukić, T., Bjelajac, D., Fitzsimmons, K.E., Marković, S.B., Basarin, B., Mlađan, D., Micić, T., Schaetzl, R.J., Gavrilov, M.B., Milanović, M., Létal, A., Samardžić, I., 2018b. Factors triggering landslide occurrence on the Zemun loess plateau, Belgrade area, Serbia. Environ. Earth Sci. 77 https://doi.org/10.1007/s12665-018-7712-z.
Lukić, T., Leščešen, I., Sakulski, D., Basarin, B., Jordaan, A., 2016. Rainfall erosivity as an indicator of sliding occurrence along the southern slopes of the bačka loess plateau: A case study of the kula settlement, vojvodina (North Serbia). Carpathian J. Earth Environ. Sci. 11, 303–318.
Lukić, T., Lukić, A., Basarin, B., Ponjiger, T.M., Blagojević, D., Mesaroš, M., Milanović, M., Gavrilov, M., Pavić, D., Zorn, M., Morar, C., Janićević, S., 2019. Rainfall erosivity and extreme precipitation in the Pannonian basin. Open Geosci. 11, 664–681. https://doi.org/10.1515/geo-2019-0053.
Luković, J., Blagojevć, D., Kilibarda, M., Bajat, B., 2015. Spatial pattern of North Atlantic Oscillation impact on rainfall in Serbia. Spat. Stat. 14, 39–52. https://doi.org/10.1016/j.spasta.2015.04.007.
Martin-Vide, J., 2004. Spatial distribution of a daily precipitation concentration index in peninsular Spain. Int. J. Climatol. 24, 959–971. https://doi.org/10.1002/joc.1030.
Masaki, Y., Hanasaki, N., Takahashi, K., Hijioka, Y., 2014. Global-scale analysis on future changes in flow regimes using Gini and Lorenz asymmetry coefficients. Water Resour. Res. 50, 4054–4078. https://doi.org/10.1002/2013WR014266.
Meusburger, K., Steel, A., Panagos, P., Montanarella, L., Alewell, C., 2012. Spatial and temporal variability of rainfall erosivity factor for Switzerland. Hydrol. Earth Syst. Sci. 16, 167–177. https://doi.org/10.5194/hess-16-167-2012.
Mishra, A.K., Özger, M., Singh, V.P., 2009. An entropy-based investigation into the variability of precipitation. J. Hydrol. 370, 139–154. https://doi.org/10.1016/j.jhydrol.2009.03.006.
Mishra, S., Ayyub, B.M., 2019. Shannon Entropy for Quantifying Uncertainty and Risk in Economic Disparity. Risk Anal. 39, 2160–2181. https://doi.org/10.1111/risa.13313.
Monjo, R., Martin-Vide, J., 2016. Daily precipitation concentration around the world according to several indices. Int. J. Climatol. 36, 3828–3838. https://doi.org/10.1002/joc.4596.
Nearing, M.A., Yin, S.-Q., Borrelli, P., Polyakov, V.O., 2017. Rainfall erosivity: An historical review. Catena 157, 357–362. https://doi.org/10.1016/j.catena.2017.06.004.
Panagos, P., Ballabio, C., Borrelli, P., Meusburger, K., 2016a. Spatio-temporal analysis of rainfall erosivity and erosivity density in Greece. Catena 137, 161–172. https://doi.org/10.1016/j.catena.2015.09.015.
Panagos, P., Ballabio, C., Borrelli, P., Meusburger, K., Klik, A., Rousseva, S., Tadić, M.P., Michaelides, S., Hrabalíková, M., Olsen, P., Beguería, S., Alewell, C., 2015a. Rainfall erosivity in Europe. Sci. Total Environ. 511, 801–814. https://doi.org/10.1016/j.scitotenv.2015.01.008.
Panagos, P., Ballabio, C., Meusburger, K., Spinoni, J., Alewell, C., Borrelli, P., 2017. Towards estimates of future rainfall erosivity in Europe based on REDES and WorldClim datasets. J. Hydrol. 548, 251–262. https://doi.org/10.1016/j.jhydrol.2017.03.006.
Panagos, P., Borrelli, P., Poesen, J., Ballabio, C., Lugato, E., Meusburger, K., Montanarella, L., Alewell, C., 2015b. The new assessment of soil loss by water erosion in Europe. Environ. Sci. Policy 54, 438–447. https://doi.org/10.1016/j.envsci.2015.08.012.
Panagos, P., Borrelli, P., Spinoni, J., Ballabio, C., Meusburger, K., Beguería, S., Klik, A., Michaelides, S., Petan, S., Hrabalíková, M., Banasik, K., Alewell, C., 2016b. Monthly rainfall erosivity: Conversion factors for different time resolutions and regional assessments. Water (Switzerland) 8. https://doi.org/10.3390/w8040119.
Petek, M., Mikoš, M., Bezak, N., 2018. Rainfall erosivity in Slovenia: Sensitivity estimation and trend detection. Environ. Res. 167, 528–535. https://doi.org/10.1016/j.envres.2018.08.020.
Rajah, K., O'Leary, T., Turner, A., Petrakis, G., Leonard, M., Westra, S., 2014. Changes to the temporal distribution of daily precipitation. Geophys. Res. Lett. 41, 8887–8894. https://doi.org/10.1002/2014GL062156.
Rajaram, R., Castellani, B., Wilson, A.N., 2017. Advancing Shannon entropy for measuring diversity in systems. Complexity 2017. https://doi.org/10.1155/2017/8715605.
Renard, K.G., Foster, G.R., Weesies, G.A., McCool, D.K., Yoder, D.C., 1997. Predicting Soil Erosion byWater: A Guide to Conservation Planning with the Revised Universal Soil Loss Equation (RUSLE) (Agricultural Handbook 703).
Rodrigues da Silva, V.D.P., Belo Filho, A.F., Rodrigues Almeida, R.S., de Holanda, R.M., da Cunha Campos, J.H.B., 2016. Shannon information entropy for assessing space-time variability of rainfall and streamflow in semiarid region. Sci. Total Environ. 544, 330–338. https://doi.org/10.1016/j.scitotenv.2015.11.082.
Rodrigues da Silva, V.P., Belo Filho, A.F., Singh, V.P., Almeida, R.S.R., Silva, B.B., de Sousa, I.F., Holanda, R.M., 2017. Entropy theory for analysing water resources in northeastern region of Brazil. Hydrol. Sci. J. 62, 1029–1038. https://doi.org/10.1080/02626667.2015.1099789.

Royé, D., Martin-Vide, J., 2017. Concentration of daily precipitation in the contiguous United States. Atmos. Res. 196, 237–247. https://doi.org/10.1016/j.atmosres.2017.06.011.
Sangüesa, C., Pizarro, R., Ibañez, A., Pino, J., Rivera, D., García-Chevesich, P., Ingram, B., 2018. Spatial and temporal analysis of rainfall concentration using the Gini Index and PCI. Water (Switzerland) 10. https://doi.org/10.3390/w10020112.
Shannon, C.E., 1948. A Mathematical Theory of Communication. Bell Syst. Tech. J. 27, 379–423. https://doi.org/10.1002/j.1538-7305.1948.tb01338.x.
Shi, W., Yu, X., Liao, W., Wang, Y., Jia, B., 2013. Spatial and temporal variability of daily precipitation concentration in the Lancang River basin. China. J. Hydrol. 495, 197–207. https://doi.org/10.1016/j.jhydrol.2013.05.002.
Signorell, A., 2020. DescTools: Tools for Descriptive Statistics.
Sun, Q., Miao, C., Duan, Q., 2017. Changes in the spatial heterogeneity and annual distribution of observed precipitation across China. J. Clim. 30, 9399–9416. https://doi.org/10.1175/JCLI-D-17-0045.1.
Tarsitano, A., 1988. Measuring the asymmetry of the Lorenz curve. Ric. Econ. 42, 507–519.
Vallebona, C., Pellegrino, E., Frumento, P., Bonari, E., 2015. Temporal trends in extreme rainfall intensity and erosivity in the Mediterranean region: a case study in southern Tuscany, Italy. Clim. Change 128, 139–151. https://doi.org/10.1007/s10584-014-1287-9.
Wieland, T., 2019. {REAT}: A {R}egional {E}conomic {A}nalysis {T}oolbox for {R}. REGION 6, R1–R57.
Wischmeier, W.H., Smith, D.D., 1978. Predicting rainfall erosion losses: a guide to conservation planning [USA]. United States. Dept. Agric. Agric. Handb.
Yin, S., Nearing, M.A., Borrelli, P., Xue, X., 2017. Rainfall erosivity: An overview of methodologies and applications. Vadose Zo. J. 16 https://doi.org/10.2136/vzj2017.06.0131.
Yin, Y., Xu, C.-Y., Chen, H., Li, L., Xu, H., Li, H., Jain, S.K., 2016. Trend and concentration characteristics of precipitation and related climatic teleconnections from 1982 to 2010 in the Beas River basin, India. Glob. Planet. Change 145, 116–129. https://doi.org/10.1016/j.gloplacha.2016.08.011.
Zabret, K., Rakovec, J., Šraj, M., 2018. Influence of meteorological variables on rainfall partitioning for deciduous and coniferous tree species in urban area. J. Hydrol. 558, 29–41. https://doi.org/10.1016/j.jhydrol.2018.01.025.
Zeileis, A., Kleiber, C., 2014. ineq: ineq: Measuring Inequality, Concentration, and Poverty.